

Statistical investigation of IMF B_z effects on energetic (0.1- to 16-keV) magnetospheric O^+ ions

O. W. Lennartsson

Research and Development, Lockheed Martin Missiles and Space, Palo Alto, California

Abstract. More than 2 years of magnetospheric O^+ data from the Plasma Composition Experiment on the ISEE 1 spacecraft are compared, in a statistical manner, with concurrent data on the interplanetary magnetic field (IMF) and the solar wind plasma in an attempt to clarify the geophysical responses to varying solar wind inputs, in particular to variations in the GSM B_z component of the IMF. It is found that the energy density of 0.1- to 16-keV O^+ ions in the plasma sheet, inside of $23 R_E$, is well correlated with the average solar wind energy flux during the preceding few hours, whether that flux is measured by its electromagnetic (Poynting) component P or by its far greater kinetic component K . Although P and K are well correlated with each other, the correlation of the O^+ energy density is slightly better with K than with P during times of positive B_z , while the opposite holds for negative B_z . In either case the O^+ energy density is more nearly proportional to K , and, given a typical value of K , there is at most a marginal (less than a factor of 2) increase in this density associated with a negative B_z . Except for this latter effect, which can perhaps be taken as evidence that a change in polarity of B_z from positive to negative may induce "unloading" of internal tail energy, there is no evidence in these O^+ data, including data from the inner magnetosphere ($L < 10$), that a negative, or southward, B_z is inherently favorable to the transfer of solar wind power across the magnetopause. These findings, together with the results of correlating the hourly AE index with P and K , suggest that the strong dependence of the AE on the B_z polarity is substantially exaggerated by the lack of AE magnetometers above 71° magnetic latitude.

1. Introduction

Although there is plentiful experimental evidence today that energetic O^+ ions of terrestrial origin generally increase in abundance throughout the magnetosphere during geomagnetic storms and substorms [e.g., Shelley *et al.*, 1972; Ghielmetti *et al.*, 1978; Balsiger *et al.*, 1980; Sharp *et al.*, 1981; Lundin *et al.*, 1982; Young *et al.*, 1982; Lennartsson and Shelley, 1986; Mobius *et al.*, 1987; Gloeckler and Hamilton, 1987; Daglis *et al.*, 1994], it is not yet clear what the physical connection really is between the O^+ and the geomagnetic disturbances. One reason for uncertainty is the large statistical variance usually obtained when correlating the O^+ density with standard geophysical indices, such as the D_{ST} , Kp , or AE [e.g., Young *et al.*, 1982; Lennartsson and Shelley, 1986]. Another reason is that the O^+ in some ways responds differently to changing solar wind conditions than do these indices, as found by Lennartsson [1991]. The latter study showed, in particular, that the density of 0.1- to 16-keV O^+ ions in the central plasma sheet, at a geocentric distance of 10 to $23 R_E$, does not have the same distinct asymmetry as the AE index when ordered by the north-south component of the solar wind magnetic field, that is, by the interplanetary magnetic field (IMF) B_z component in geocentric solar magnetospheric (GSM) coordinates. While the O^+ density and the (hourly) AE were both found to increase with an increasing value of the recent IMF magnitude, whether B_z is positive or negative, only the AE showed a significantly

larger increase with a negative B_z (by about a factor of 2-3; see Figure 4 of Lennartsson [1991]).

This study is a follow-on to Lennartsson [1991], using a more extensive set of data and data with substantially improved time resolution. Like the earlier study it uses magnetospheric O^+ data obtained by the Lockheed Plasma Composition Experiment on the International Sun-Earth Explorer One (ISEE 1) spacecraft [Shelley *et al.*, 1978], complemented with geomagnetic field data from another experiment on that same spacecraft [Russell, 1978] and concurrent solar wind plasma (protons) and magnetic field (IMF) data extracted from the National Space Science Data Center (NSSDC) OMNI file [Couzens and King, 1986].

In order to place the following analysis in the proper context, it is helpful to restate four specific results from the earlier study, all based on statistical averaging and referring to the number density of 0.1- to 16-keV O^+ ions in the central plasma sheet:

1. The O^+ density increases with increasing solar wind ram pressure, that is, with an increasing value of the product between the solar wind density and the square of the solar wind flow speed, but it appears to respond more strongly to a given relative increase in the latter factor, when those two factors are considered separately.

2. It also increases with increasing angle between the IMF vector \mathbf{B} and the solar wind velocity vector \mathbf{v} , being the largest when \mathbf{B} and \mathbf{v} are perpendicular.

3. Apart from a low ($\sim 0.02 \text{ cm}^{-3}$) quiet-time value, it is approximately proportional to the square of the solar wind electric field, that is, to $E_{\text{sw}}^2 = |\mathbf{v} \times \mathbf{B}|^2$, whether \mathbf{v} and \mathbf{B} are measured during the same time interval as the O^+ or during

Copyright 1995 by the American Geophysical Union.

Paper number 95JA02859.
0148-0227/95/95JA-02859\$05.00

the immediately preceding hour. The same dependence is also displayed by the O^+ energy density.

4. It does not show a significant dependence on the rotation angle of E_{sw} around v .

Because of 1, 2, and 3, and in spite of 4, it was concluded, possibly prematurely, that the electric field E_{sw} is the principal medium for transfer of energy between the solar wind and the magnetospheric O^+ population.

The last of these four results is intriguing, not only because of a possible conflict with the interpretation of the other three but also because it defies the popular notion that solar wind power becomes much more easily transferred across the magnetopause when the IMF turns from northward to southward. Despite its important implications it was not thoroughly tested in the original study, because the O^+ data format available at that time was deemed inadequate. It was noted, in particular, that the number density of ions in the plasma sheet is not, by itself, a reliable measure of the rate of emission of ions from Earth's atmosphere; it is conceivable that increased emission at polar latitudes during times of southward IMF does not produce a net increase in the density at equatorial latitudes, beyond $10 R_E$, because it is offset by increased ion loss through Earthward convection. The data format offered no ready means to directly measure the outflow of O^+ ions along the geomagnetic field lines, and the data available from the inner magnetosphere were too limited to really test whether the O^+ density increases there specifically because the IMF stays southward. Furthermore, the poor time resolution of the velocity moments, between 1 and 3 hours in the plasma sheet, made it difficult to associate the O^+ data with the proper hour, or hours, in the OMNI file.

This study is based on a new set of O^+ data with a more suitable format, obtained by reprocessing 28 months of raw data from the ISEE 1 experiment. As a further refinement this study focuses on the actual energy flows in the solar wind, rather than the associated forces. The new results essentially confirm all four listed above, but they provide a different perspective on the physical interpretation, especially when they are compared with parallel results of a correlation of the AE index with solar wind energy flows. The upshot is that the solar wind ram pressure probably plays a more prominent role than originally thought.

2. Database

2.1. Magnetospheric O^+ Data

The Lockheed Plasma Composition Experiment on the ISEE 1 spacecraft [Shelley *et al.*, 1978] measures ions at various mass per charge (M/Q) in a cyclic fashion, usually by scanning the full range of energy per charge (E/Q) while maintaining a fixed M/Q . Each E/Q setting is typically kept fixed for at least one full spacecraft spin period (3 s). A complete energy-mass scan cycle in the magnetospheric modes of operation usually requires about 8–17 min. This instrument cycle defines the time resolution of these data, in contrast to the earlier data set, which was based on 1- to 3-hour averages of the count rates in various energy and angle bins [see Lennartsson and Shelley, 1986]. Each cycle includes an M/Q setting (<1) which provides direct measurements of detector noise due to penetrating high-energy radiation (mostly bremsstrahlung associated with MeV electrons). This background is subtracted from the other measurements before converting counts to velocity moments.

In addition to the mass-analyzed counts the instrument also

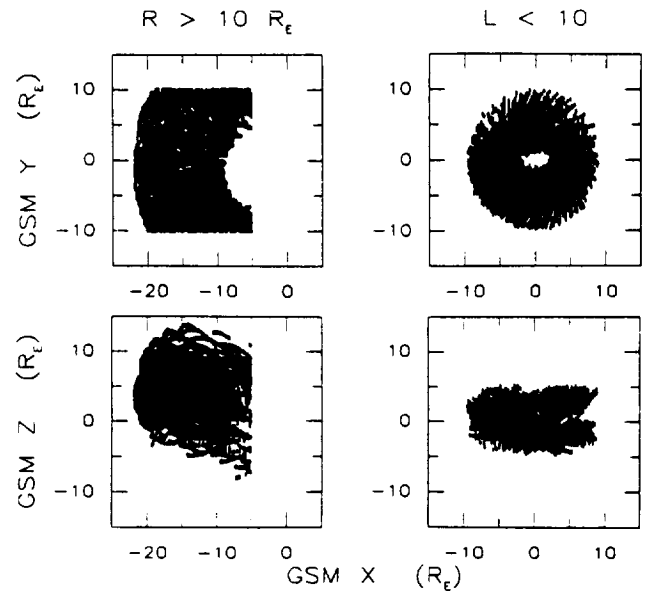


Figure 1. Spatial extent of selected O^+ data from (left) central tail and (right) inner magnetosphere, displayed in geocentric solar magnetospheric (GSM) coordinates. Points in right panels are delimited by dipole L (see text).

returns a total ion count rate (at a given E/Q) from a separate detector. This latter count rate can be converted to velocity moments after each energy-spin-angle cycle, if it is assumed to represent H^+ ions only.

The present O^+ data cover for the most part the E/Q range between 100 eV/e and 16 keV/e, when in the form of velocity moments, but some flux data covering the larger range of 10 eV/e to 18 keV/e are also considered. The ion data are supplemented with magnetic field data from the ISEE 1 Fluxgate Magnetometer [Russell, 1978]. Both kinds of data are taken from a large set of archival data recently delivered to the NSSDC (indexed as 77-102A-121). The data format is described in some detail in the appendix section of another recent study by this author [Lennartsson, 1994]. That same reference also has a more complete description of the instrument. A complete data format description is presently available electronically via Internet Netscape, along with a sample subset of the data, on the WWW page <http://ftp.sierra.space.lockheed.com/DATA/isee/Welcome.html>.

For this study the data set has been spatially limited to two different regions, as illustrated in Figure 1, one being the "central tail," defined according to the left panels, the other the "inner magnetosphere," defined according to the right panels. Each point in Figure 1 represents a single energy-mass scan cycle of the instrument, that is, a single mass-resolved plasma sample. The tail region lies at GSM R between 10 and $23 R_E$, the latter being the ISEE 1 apogee, and at $X < -5 R_E$ and $-10 R_E < Y < 10 R_E$. The bias toward positive Z is a consequence of the ISEE 1 orbit. The L value used to delimit the inner magnetosphere in the right panels is a simple centered-dipole L , defined as the geocentric distance in units of R_E , divided by the square of the cosine of the magnetic latitude of ISEE 1. The particular choice of outer L boundary is explained later. The data span a total time period from November 8, 1977, through March 1, 1980.

The tail data have been further subdivided according to ion

density and magnetic field strength into tail lobe and plasma sheet, specifically "central plasma sheet." The latter has been defined by the following conditions:

1. The sum of the H^+ , He^{++} , He^+ , and O^+ densities is at least 0.1 cm^{-3} .
2. The plasma beta value produced by these same ions is at least 0.1.
3. The multiple (typically 5–8) density values derived from the "total ion" count rates during the course of each energy-mass scan cycle, assuming only H^+ ions, are all at least 0.05 cm^{-3} .

These conditions differ slightly from those used by Lennartsson [1991] but lead to essentially the same selection within the GSM boundaries imposed in the left panels of Figure 1. These boundaries are somewhat arbitrary, although they do encompass the region of maximum O^+ concentration in the tail [Lennartsson and Shelley, 1986] and also the region where the ISEE 1 spacecraft provides comparable sampling of the plasma sheet and the tail lobes (mostly the northern lobe). Outside of this region, at $|Y| > 10 R_E$, the plasma sheet is often too thick (in the Z direction) to allow sampling of the lobes, especially during geomagnetically quiet periods.

In addition to the spatial constraints of Figure 1, the data have been screened by the analysis program for evidence that the ISEE 1 may have been in the magnetosheath or in the solar wind, and data have been discarded on a conservative basis. This screening has been based on velocity moments, combining the mass-resolved H^+ and He^{++} moments as well as the "total ion" moments, assuming that the latter are well representative of H^+ ions.

2.2. Solar Wind Data

The solar wind data are a combination of particle and magnetic field (IMF) data from several different instruments and spacecraft, compiled as hourly averages into a single electronic digital file ("OMNI") by Couzens and King [1986]. This file, which covers many years of solar wind observations (from 1963 onward), has been furnished by the NSSDC in the standard magnetic-tape version (37 words per record and in ASCII).

The original data were either obtained in the close vicinity of Earth's magnetopause (within a few tens of R_E), or they were time shifted according to the observed solar wind flow before insertion in the file (applied to data from ISEE 3 [see Couzens and King, 1986]). The particle data represent protons, having the form of a flowing Maxwell-Boltzmann distribution with the flow velocity specified in geocentric solar ecliptic (GSE) coordinates. The IMF is specified in both GSE and GSM coordinates. Particle and IMF data are both available from this file in conjunction with about 70% of the ISEE 1 O^+ measurements in Figure 1.

3. Statistical Results

3.1. Differential (Tailward) Flux of O^+ Ions

It is natural to begin this study where the previous one ended [Lennartsson, 1991], namely with the question whether the rate of emission of energetic O^+ ions from Earth's atmosphere does or does not depend on the polarity of the IMF B_z . The new data set offers a more direct means to measure the emission, namely with the help of files of peak count rates, or peak differential fluxes (see section A2 of Lennartsson [1994]). The fluxes considered here are those of ions reaching beyond $10 R_E$ in the tail; ions which do not reach that far, because of equa-

ward and Earthward convection, will to some extent be accounted for in a later section about the inner magnetosphere.

Figure 2 shows the average peak flux of O^+ ions in the tail region (left panels of Figure 1) as a function of the measured local ion beta during conditions of northward (left) and southward (right) IMF. In the top panels the IMF status refers to the current hour (universal time), that is, the hour in which the O^+ was sampled in the tail; in the bottom panels it refers to the immediately preceding hour. Very similar results are obtained with a delay of 2 or 3 hours (not shown). The beta has been calculated under the second set of assumptions stated in section A2 of Lennartsson [1994] (see also discussion of beta on page 2388 of that paper) and combines the perpendicular pressures of H^+ , He^{++} , He^+ , and O^+ ions.

The reason for sorting the O^+ data according to beta is to minimize the possible bias from a spatial redistribution of the plasma sheet and the tail magnetic field between times of northward and southward IMF. It is clear from the data (not shown) that the ISEE 1 spends a greater portion of the time under conditions of low plasma density and low beta during times of southward IMF. This is due in part to a reduced total ion density (see Figures 5 and 6 of Lennartsson [1992] in regard to H^+ and He^{++} densities) and in part, probably, to a local increase of the magnetic field strength in association with a more dipolelike tail field [e.g., Fairfield and Ness, 1970]. Using beta as the "spatial" coordinate here should therefore help compensate for a systematic displacement of particle trajectories that may result from faster equatorward and Earthward convection.

The O^+ data in Figure 2 have been limited to samplings with full pitch-angle coverage at all energies, that is, samplings with minimum and maximum center pitch angles of less than 5° and greater than 175° , respectively (see section A1 of Lennartsson [1994]). The peak flux is usually (almost always at low beta) associated with O^+ ions flowing in the antisunward direction, that is, tailward, and it often occurs in the lowest energy channel or the next to lowest one, that is, at energies from 10 eV to about 300 eV, especially at low beta. If count rates are restricted to 10 or more per sampling (about 40 per second in normal low bit rate), as done by Sharp *et al.* [1981] in order to ensure statistical significance, about 70% to 80% of the peak fluxes at beta < 0.1 are found within $\pm 30^\circ$ of the tailward magnetic-field direction, counted in the spin plane, and as much as 90% if beta is restricted to < 0.01 , although the angular resolution of the instrument is insufficient (effectively about $\pm 20^\circ$ in low bit rate) to make precise estimates.

With count rates still restricted to 10 or more per sampling the average energy in keV at peak flux in each of the four bins of ion beta, from low to high beta, is approximately 0.24, 0.80, 1.10, and 2.22 in the left panels (top and bottom averaged) and 0.29, 1.42, 1.84, and 2.93 in the right panels. That is, the peak O^+ flux, in that case, occurs at roughly 50% higher energy during southward IMF.

As Figure 2 shows, the O^+ tends to have a higher peak differential flux at lower beta in the tail. This merely reflects a greater degree of collimation of the flux there, both in angle and energy [Sharp *et al.*, 1981], and it contrasts with the O^+ number density, which is greater, in absolute terms, at higher beta [Lennartsson, 1994]. This situation is consistent with the O^+ at low beta and low energy being a source for the more isotropic and hotter O^+ at high beta, if only a partial source.

According to Figure 2, the source feeding O^+ ions to the

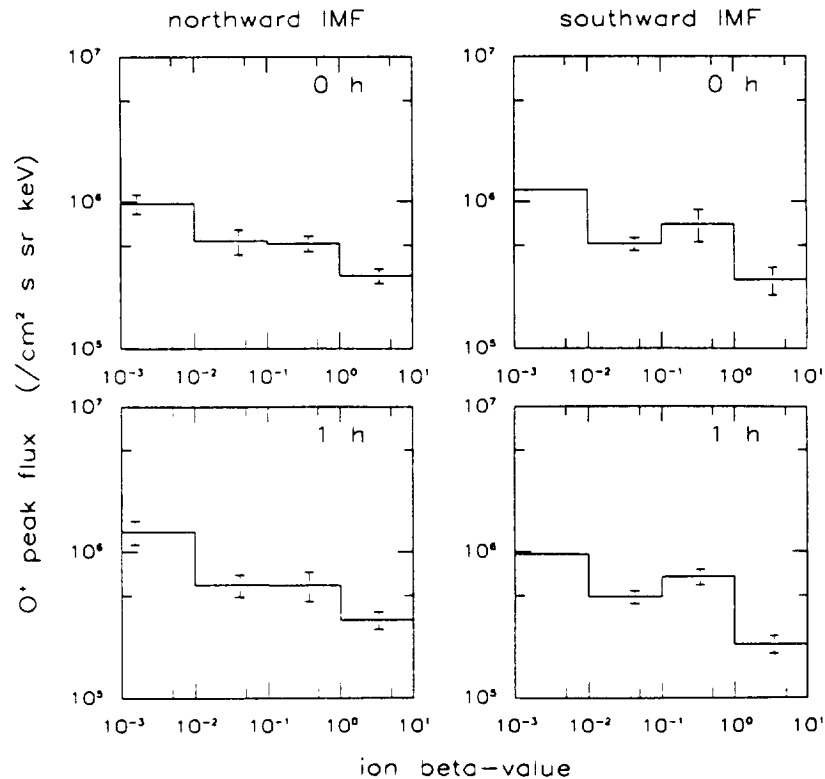


Figure 2. Averages of peak differential O^+ flux in each energy-angle scan by instrument in central tail, sorted by decades of total ion beta (including the four principal ion species; see text) and by the direction of the hourly IMF B_z (north or south) during (top) present hour or (bottom) immediately preceding hour. Peak flux is anywhere in the 10-eV to 18-keV range but mostly below a few keV and is mostly directed tailward (see text for details). Error bars in this and following figures show standard deviation of the average in each bin ($\pm 1\sigma$), as calculated from available data points, and are placed at the average abscissa of all points in the bin. These bars are displayed only when relative error is larger than 10%.

plasma sheet, via low or high beta field lines, is about equally strong, within one or two standard deviations of mean flux (shown by error bars), whether the IMF is northward or southward (averaged over IMF magnitude). This may seem counterintuitive, but it is again consistent with the O^+ density being about equal. The largest O^+ fluxes tend to occur at somewhat higher energy with a southward IMF, as indicated above, but the net cumulative effect over an hour or longer is not sufficient to produce a correspondingly greater mean energy of O^+ ions in the plasma sheet. In fact, the mean energy is some 15% lower with a southward IMF. This topic will be revisited below. For comparison, the grand average hourly AE during all O^+ samplings in the upper left panel of Figure 2, excluding some that were obtained in 1977 when no AE index was available, was 156 nT, and the corresponding average for the upper right panel was 367 nT, or more than twice as large. The respective AE values for the lower panels were almost identical (slightly different sets of hours, subject to the availability of IMF data).

Somewhat similar results have been obtained closer to Earth as well, but the pitch-angle coverage of the ISEE 1 data at low L is insufficient to provide conclusive evidence about field-aligned flows there (section A1 of Lennartsson [1994]).

3.2. Number Density of O^+ Ions in the Central Plasma Sheet

As noted in the previous study the O^+ ions in the plasma sheet in some ways appear to be controlled by the partial

energy flux, or “Poynting flux,” associated with the solar wind electric and magnetic fields. This interpretation was based mainly on the good correlation between the O^+ density and the square of the solar wind electric field (point 3 in section 1), but a direct correlation with the energy flux had not been attempted prior to this study.

The electric field $\mathbf{E}_{sw} = -\mathbf{v} \times \mathbf{B}$ does combine with the IMF to form a Poynting vector $\mathbf{E}_{sw} \times \mathbf{B}/\mu_0$ (μ_0 being the permeability of vacuum in MKS units), but, as is often the case when this vector is derived from near-static fields, its physical meaning becomes somewhat obscure. It has been assumed here that only the component along the solar wind bulk velocity vector \mathbf{v} is a relevant measure of true energy flow. This component may be written as

$$P = \mathbf{E}_{sw}^2 / (\mu_0 |\mathbf{v}|) \quad (1)$$

The vector \mathbf{v} used in this study is measured relative to Earth. The orbital motion of Earth around the Sun is accounted for by an average speed of 29.8 km/s added to the GSE Y component from the OMNI file, which is aberration corrected (the orbital speed varies only slightly, between 29.3 and 30.3 km/s).

It may be noted that \mathbf{E}_{sw} is by far the most strongly varying parameter on the right side of (1), due to variations in the direction and magnitude of the IMF (compare IMF and solar wind flow data of Couzens and King [1986]), so P is in effect roughly proportional to \mathbf{E}_{sw}^2 . This was presumed to be the

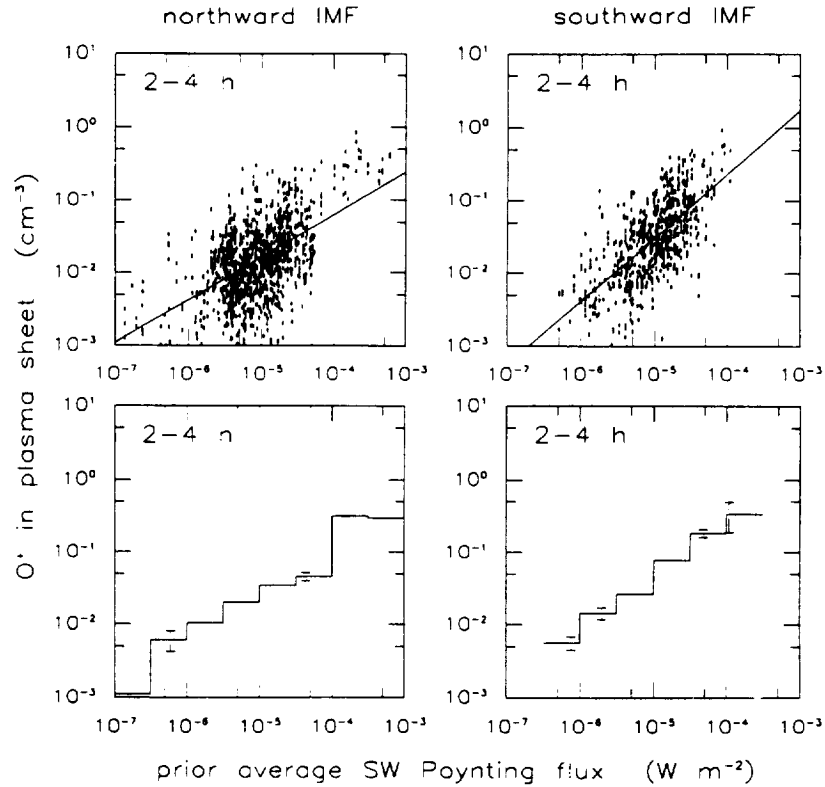


Figure 3. (top) Scatter plots of 0.1- to 16-keV O^+ density in the plasma sheet (defined in text) as a function of the average solar wind Poynting flux P (see text) during the 3-hour interval ending with the second most recent hour, counting the present hour as #0 and requiring that the IMF B_z remain consistently either (left) northward or (right) southward during that interval. The respective regression line has correlation coefficient (left) $r = 0.55$ and (right) $r = 0.68$. The corresponding number of O^+ samplings is (left) $N = 1150$ and (right) $N = 672$. The least squares fits here and in following figures are unweighted (see text). (bottom) Same data binned and averaged (showing standard deviation of mean).

underlying reason for the average parabolic relationship found previously between E_{sw} and the O^+ density.

Since P in (1) is a rate of energy flow, its effect on terrestrial O^+ ions must be cumulative, up to some limit set by ion loss processes. This is to some extent already accounted for by the fact that P is based on hourly averages of solar wind parameters here, but further averaging over a few hours has been found to improve its correlation with the O^+ density. A good example is shown in Figure 3.

The Poynting flux in Figure 3 has been averaged over a 3-hour interval preceding the hour during which each O^+ sampling was made, counting the latter as hour "0" (typically 3 to 5 O^+ samplings per hour, only some of which may qualify as "plasma sheet"). Only those data points which had the three hourly IMF B_z values consistently either positive (left panels) or negative (right panels) have been included. This accounts in part for the large reduction in data points compared to the left panel of Figure 1. The other limiting factor is the requirement that each sampling represents the central plasma sheet, as defined in section 2.1 above, which is especially restrictive during times of southward IMF (lower plasma density or lower beta; right panels).

Before the regression lines in Figure 3 are appraised, it is probably appropriate to consider the applicability of least squares fitting. This method assumes that the scatter in the y variable about some average relationship $y = f(x)$ obeys a Gaussian, or normal, distribution. To the extent that the scat-

ter in the O^+ number density is caused by counting statistics, it should indeed be well approximated by such a distribution (asymptotic limit of a Poisson distribution for a large sum of counts [e.g., *Bevington*, 1969, p. 77]), but the main part of the scatter is due to other and basically unknown causes, probably including spatial inhomogeneities. It is impossible to prove that this part obeys a normal distribution, but it can at least be said to have a superficially normal appearance (not shown).

When the y variable is plotted on a logarithmic scale, the scatter in y retains its "quasi-normal" appearance, except that it becomes somewhat skewed to lower values. This may have a slight biasing effect on the vertical placement of a straight-line fit to the log-log coordinates of Figure 3, as compared to fitting a relation of type $y = ax^b$ to linear coordinates, but it should not affect the comparison with other figures, since the same procedure is used everywhere. These fits are all performed without weighting in the χ^2 sum, since there is no simple means of assigning a separate sigma to each data point. Fortunately, the scatter in y on a logarithmic scale is in most cases fairly even, so a constant sigma (no weighting) may be justifiable.

The O^+ density in the plasma sheet generally correlates the best with solar wind conditions some 2 to 4 hours earlier and somewhat better with a 3-hour average of these conditions than with single hourly values. As Figure 3 shows, the O^+ is indeed well correlated with the solar wind Poynting flux, whether that is due to a direct physical link or due to a common dependence of both on some other solar wind variable.

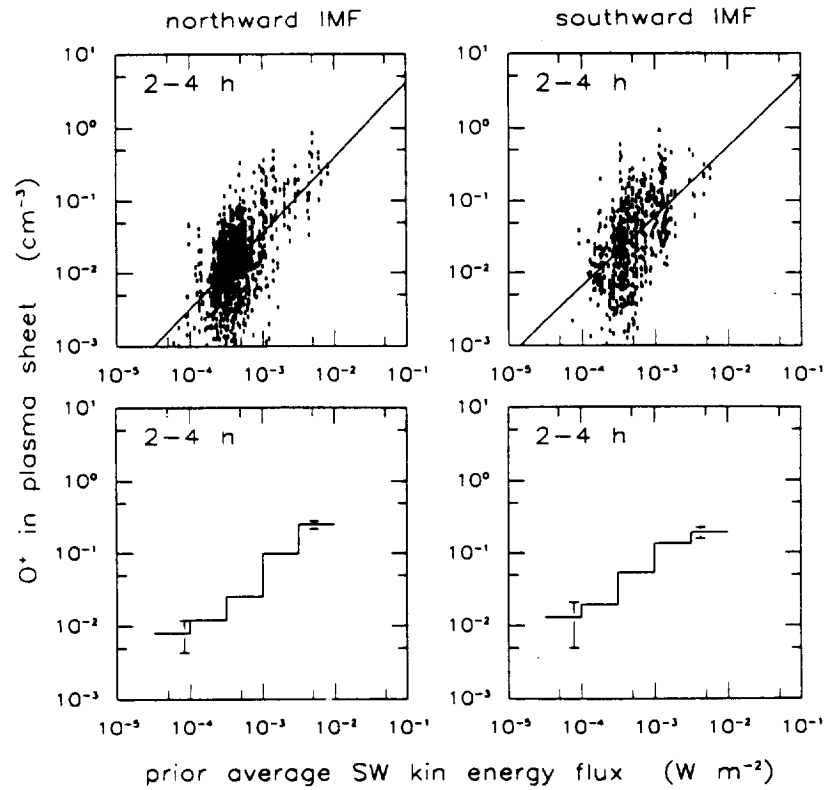


Figure 4. Same as Figure 3 but with the O^+ density sorted by the solar wind kinetic energy flux K (see text). The regression lines in the top panels have (left) $r = 0.61$ and (right) $r = 0.53$. The number of samplings in each panel is the same as in Figure 3. Note the different scale on the abscissa.

Despite the large scatter, having a correlation coefficient r as high as 0.5 to 0.7 with this many data points translates to virtual certainty. Stated differently, the probability of having no correlation under these conditions [e.g., Bevington, 1969, pp. 119–127; Press *et al.*, 1986, pp. 484–487] is so small as to fall within the rounding errors of double-precision computing ($\sim 10^{-9}$). The difference in r between the left and right panels, 0.13, is larger than can be ascribed to mere chance and implies that the correlation with P is somewhat better with a southward IMF. The right (upper) panel is also where the slope of the regression line is largest, almost 45° (tangent = 0.87 ± 0.04), indicating a nearly proportional relationship between P and the O^+ density.

The random error in r , in Figure 3 and following figures, has been estimated from comparisons between randomly selected subsets of the data to be consistently less than 0.05 and in most cases less than 0.03 (plus or minus). It may be recalled that the analytical formulas for least squares fitting do provide standard deviations for the location and slope of a regression line but do not provide that measure for the correlation coefficient r [e.g., Bevington, 1969].

With this particular sorting of the O^+ data by IMF polarity the O^+ density is actually larger on average during times of southward IMF but only marginally so. Specifically, the grand average O^+ density in the right panels of Figure 3 is $0.061 \pm 0.003 \text{ cm}^{-3}$, roughly 80% higher than the corresponding value of $0.033 \pm 0.002 \text{ cm}^{-3}$ in the left panels. This difference is certainly small compared to the order-of-magnitude variations within each panel. Furthermore, since the plasma sheet is spatially thinner with a southward IMF (see comments in pre-

ceding section), it is not clear that the total number of O^+ ions in the tail is at all larger. By comparison, the grand average hourly AE values during O^+ samplings in the right and left panels (excluding 1977) were 413 nT and 97 nT, respectively, that is, the AE was typically more than 4 times higher for southward IMF conditions. The AE is, however, better correlated with solar wind conditions during the most recent 1 or 2 hours, which will be discussed later.

Although the solar wind Poynting flux is sufficiently strong by itself to easily account for the energy content of plasma sheet O^+ ions [Lennartsson, 1991], by far the largest portion, typically about 98%, of the solar wind energy flux is in the material, or kinetic, form. If the O^+ were well correlated with this form of energy flux, then the first of the four results listed in the introduction would have a simple explanation: it is not the square of the solar wind speed that is the relevant parameter, but rather the cube of the speed, and it did have about the same dynamic range as the solar wind density in those data (see Figures 3 and 6 of Lennartsson [1991]). To address this issue, it has been assumed here that the solar wind kinetic energy flux K in Earth's frame is that of a flowing Maxwell-Boltzmann distribution of protons [e.g., Longmire, 1963, p. 22],

$$K = nm|\mathbf{v}|^3/2 + 5nkT|\mathbf{v}|/2 \quad (2)$$

where m is the proton mass and n , $|\mathbf{v}|$, and kT are the hourly averaged proton density, bulk flow speed, and thermal energy extracted from the OMNI file (flow speed modified to include Earth's orbital motion), respectively. The second term on the right typically contributes no more than 1–2% of the sum.

Figure 4 is analogous to Figure 3 with K substituted for P

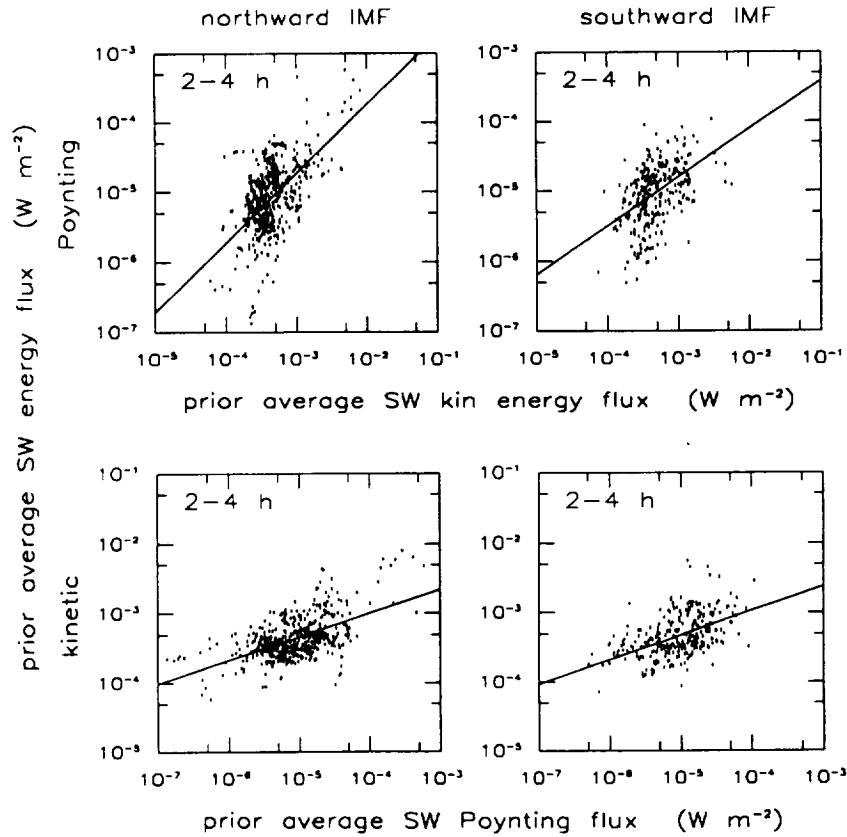


Figure 5. Intercomparison of all 3-hour averages of P and K used in Figures 3 and 4. Regression lines have (left) $r = 0.58$ and (right) $r = 0.50$ (top and bottom panels have same r by definition). Corresponding number of samplings is (left) $N = 637$ and (right) $N = 395$.

and with a different scale on the abscissa. The degree of correlation is quite comparable, and there is again a small but probably significant difference in r between the left and right panels, namely 0.08 (random error estimated to be less than ± 0.03). This time the correlation is better with a northward IMF, however. Although this difference between northward and southward IMF conditions is marginal, it does persist if the time averaging of K is varied somewhat or if a recent single hourly value is used instead (not shown). The slope of the regression line is also the largest with northward IMF here (tangent = 1.04 ± 0.04 in left panel), but it is still marginally larger than in Figure 3 even with a southward IMF (tangent = 0.96 ± 0.06 in right panel here). Hence the O^+ density is generally more nearly proportional to K than to P , a result which reflects the physical fact that P has a larger relative dynamic range than K . That is, with the correlation being about equal with either P or K , the regression line must be shallower with P in order to span a wider range of x coordinates.

The similarities between Figures 3 and 4 might be due, at least partly, to a mutual dependence between P and K . To examine that aspect, the 3-hour values of P and K used in Figures 3 and 4 have been correlated with each other in Figure 5, treating P as a function of K (top panels) and vice versa (bottom panels). Indeed, the degree of correlation is about the same here as in Figure 4, within the estimated random error of 0.03 in r . Although the regression lines have different slopes, the correlation coefficient r is the same in the top and bottom panels [e.g., *Bevington*, 1969, p. 120]. (This correlation between

P and K , combined with the limited number of samplings, is the basis for not performing multiple regression.)

Returning to the earlier results listed in the introduction, it may be noted that point 2 by itself is an indication, if only superficially, that the electric field $E_{sw} = -\mathbf{v} \times \mathbf{B}$ might play a crucial role in energizing the O^+ via its Poynting flux. This result was based on an average of data with both northward and southward IMF, sorted into 30° -wide bins in angle. With significantly more samplings available in the new O^+ data set, it is possible to reduce the width of the angular bins by half and to separate the data according to the polarity of IMF B_z . If the angle (acute here) is then averaged over the same 3-hour time interval used in Figures 3 and 4, the result is as shown in the top panels of Figure 6. The lower panels show the corresponding 3-hour P (middle) and K (bottom). The angle used here is the arc sine of the average of the three sine values corresponding to each set of three hourly angles. This is intended to more accurately reflect the time-averaged effect of the cross product $\mathbf{v} \times \mathbf{B}$.

One of the three quantities on the ordinate in Figure 6, namely the Poynting flux P , is a function of angle by definition, being proportional to sine square if $|\mathbf{v}|$ and $|\mathbf{B}|$ are constant (see (1)). The dependence of the O^+ density essentially confirms the earlier result. The dependence of the kinetic energy flux K on the angle between \mathbf{v} and \mathbf{B} , that is, the increase with increasing angle, is unexpected, however. Apparently, K is about 2 to 3 times larger, on average, when the angle is near 90° , as compared with 0° angle, at least when it is sampled on the basis of conditions in Earth's plasma sheet (section 2.1). This may

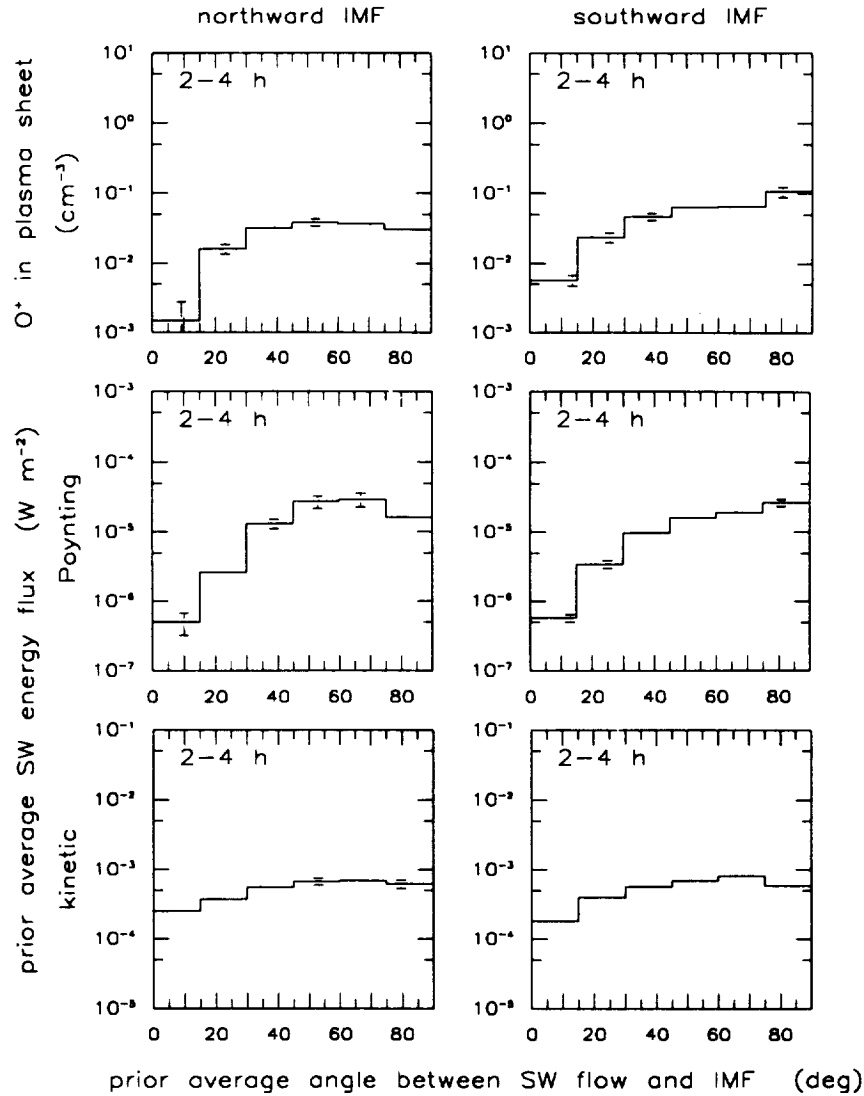


Figure 6. (top) Plasma sheet O^+ density sorted and binned according to the average angle between \mathbf{v} and \mathbf{B} during each of the 3-hour intervals used in Figures 3 and 4. (middle) Grand average P in each such bin. (bottom) Corresponding averages of K .

reflect a dependence of the angle on K , rather than the other way around, but the actual physical reason is not important here. What matters is that it may contribute to the observed dependence of the O^+ density.

The substantial reduction of the O^+ density at $<15^\circ$ in Figure 6, as compared to the 15° – 29° bin, is significant in terms of the calculated standard deviation of the mean (shown by the error bars), being about 3 times the root-mean-square value of the two sigmas at $<30^\circ$. However, the mean at $<15^\circ$ is based on only six O^+ samplings for southward IMF (right panel), taken during four different 3-hour solar wind intervals. The situation for northward IMF is somewhat better, with the mean at $<15^\circ$ being based on 22 O^+ samplings, taken during 13 different 3-hour solar wind intervals. (The small dip in some parameters near 90° is believed to be a sampling bias.)

3.3. Energy Density of O^+ Ions in the Central Plasma Sheet

In order to maintain compatible physical units, the preceding comparisons ought to have involved the energy density of

the O^+ rather than its number density. However, the two densities tend to be almost proportional to each other, because of the comparatively small variations in the O^+ mean energy, and using the number density does reduce the scatter in the data. The latter is a consequence of the fact that the O^+ data files, for certain practical reasons, do not list the energy density separately but only the ratio between energy and number densities, that is, the mean energy, a quantity that may have large absolute statistical uncertainty when densities are low (calculated composite standard deviations are listed in the data files [see Lennartsson, 1994]).

Multiplying each O^+ number density with the corresponding mean energy does, to some extent, reduce the overall correlation with solar wind conditions, thereby reducing the slope of the corresponding regression lines, but all systematic effects mentioned in section 3.2 remain qualitatively the same. This is illustrated in Figure 7 for the comparisons with P and K . The top and bottom panels of Figure 7 correspond directly to the top panels of Figures 3 and 4, respectively.

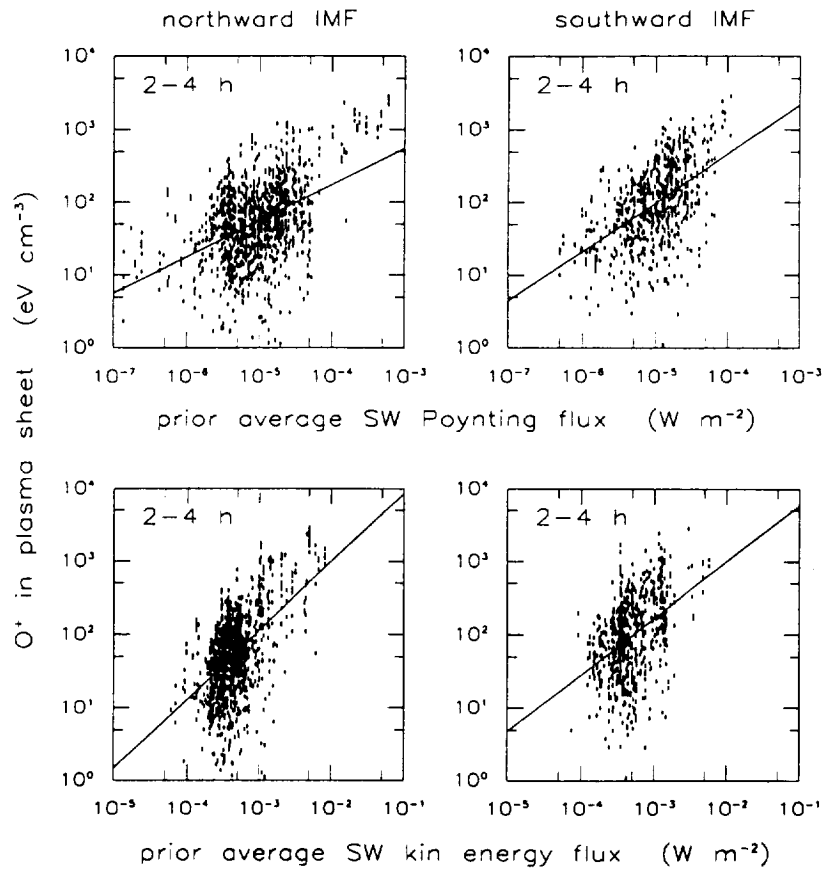


Figure 7. Same kind of scatter plots as in Figures 3 and 4 using the plasma sheet O^+ energy density rather than number density. The correlations are somewhat weaker because of greater numerical uncertainties in this density (see text). The associated statistical parameters are listed in Table 1 for later analysis.

As discussed by Lennartsson and Shelley [1986] and Lennartsson [1991], the typical plasma sheet O^+ mean energy tends to decrease slightly with increasing O^+ density, from about 5 keV at very low ($<0.01 \text{ cm}^{-3}$) density to about 3.5 keV at moderate to high density. This effect probably contributes to the somewhat shallower slope of the regression lines in Figure 7, as compared to those in Figures 3 and 4. Whether related to this effect or not, there is also a very slight reduction of the typical mean O^+ energy during southward IMF, about 15%, compared to northward IMF. As a consequence, the grand average energy densities in the left and right panels of Figure 7 differ even less than the number densities do, being $128 \pm 5 \text{ eV cm}^{-3}$ for northward IMF and $200 \pm 9 \text{ eV cm}^{-3}$, or some 60% higher, for southward IMF. The regression parameters are listed in Table 1 for later discussion.

3.4. Number Density of O^+ Ions in the Inner Magnetosphere

Comparing ion densities in the inner magnetosphere with prior solar wind conditions raises difficult questions in regard to proper timing, because of the complex and rather slow drift motion of the ions in local time, combined with ion loss. The local-time drift is especially complex in the energy range of these O^+ data, since that range encompasses both low-energy ions carried eastward by $\mathbf{E} \times \mathbf{B}$ drift and higher-energy ions moving westward by gradient B and curvature drifts, and the dividing energy (in the keV range) varies with local time and distance from Earth [e.g., McIlwain, 1972]. Energy- and angle-integrated quantities, such as number density, are therefore not as well correlated with solar wind conditions here as they

Table 1. Regression Lines $y = a + bx$ From Figure 7, With $y = \log(O^+ \text{ Energy Density})$ and $x = \log(P)$ or $x = \log(K)$

Northward IMF ($N = 1115$)		Southward IMF ($N = 658$)	
$x = \log(P)$	$x = \log(K)$	$x = \log(P)$	$x = \log(K)$
$a = 4.2 \pm 0.2$	$a = 4.9 \pm 0.2$	$a = 5.4 \pm 0.2$	$a = 4.6 \pm 0.2$
$b = 0.50 \pm 0.03$	$b = 0.94 \pm 0.05$	$b = 0.67 \pm 0.04$	$b = 0.77 \pm 0.07$
$r = 0.44$	$r = 0.52$	$r = 0.52$	$r = 0.42$

IMF is interplanetary magnetic field.

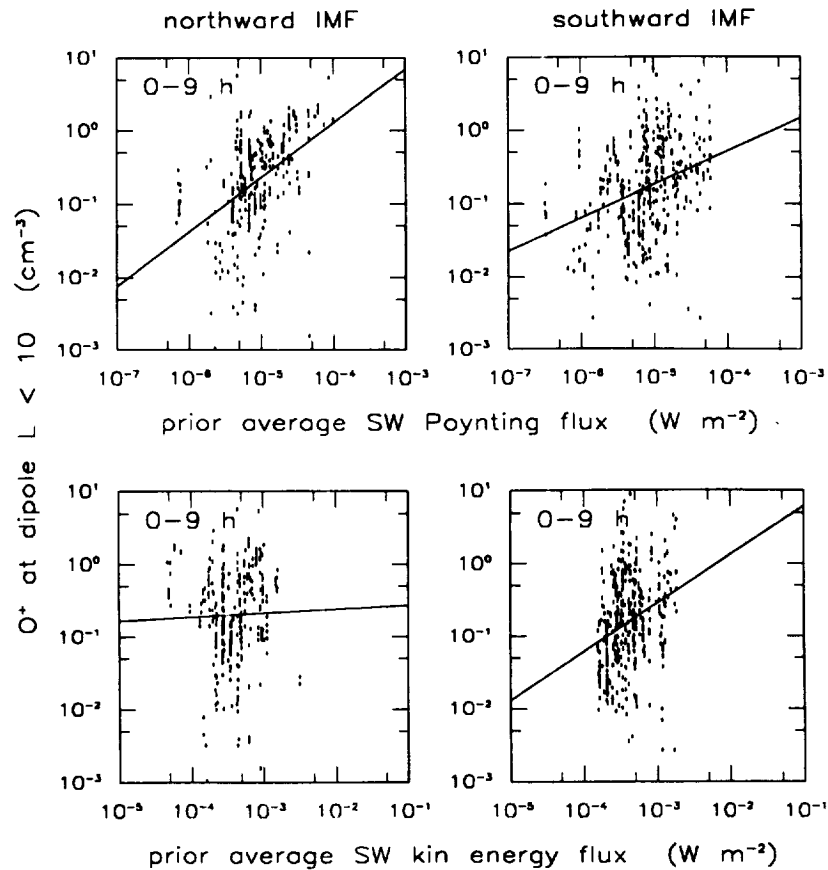


Figure 8. Scatter plots of 0.1- to 16-keV O^+ number density in “inner” magnetosphere as a function of preceding 10-hour averages of (top) P and (bottom) K , including present hour, when the hourly IMF B_z has remained either (left) northward or (right) southward for at least that long. The respective regression line has $r = 0.46$ (top left), $r = 0.34$ (top right), $r = 0.03$ (bottom left), and $r = 0.28$ (bottom right). The number of samplings are (left) $N = 304$ and (right) $N = 398$.

are in the plasma sheet. The situation is further aggravated by the need to treat all O^+ data in a large spatial region as equivalent in order to have a sufficient statistical ensemble.

This situation may justify one to focus on the most general aspects of the data and not to dwell on some peculiar details. The specific question to be addressed by this subsection is fairly general: Is there any evidence in the O^+ data from $L < 10$ that a persistently southward IMF makes the transfer of energy from the solar wind more efficient than does a persistently northward IMF?

The reason for using an outer boundary as distant as $L = 10$ is to ensure a statistically significant number of O^+ samplings even with a very restrictive definition of “persistent” solar wind conditions. The same kind of comparisons between the O^+ and the solar wind status have been made both for $L < 10$ and $L < 7$ with quite similar results, as far as these go. However, the number of samplings is reduced by a factor of 3 with the smaller region, substantially reducing the statistical significance of any correlation.

Figure 8 shows results analogous to those in the top panels of Figures 3 and 4, obtained under the requirement that as many as 10 consecutive hourly IMF B_z values remain either positive or negative prior to and including each O^+ sampling. This requirement is a somewhat arbitrary compromise between the statistical need to have enough qualifying solar wind data, that is, to keep the number of such hours within reason, and

the physical need to both maximize the cumulative effect of each IMF polarity, if there is such an effect, and allow sufficient time for the O^+ ions to disperse in local time before the next reversal of the IMF B_z . Similar results have been obtained with time intervals a few hours longer or shorter than 10 hours.

Before addressing the main issue it is worth mentioning, at least, that the O^+ density in the inner magnetosphere, as illustrated by Figure 8, is generally somewhat better correlated with the Poynting flux P than with the kinetic energy flux K , regardless of IMF polarity. In Figure 8, there is really no correlation at all with K for northward IMF, considering the modest number of samplings and the inherent uncertainty in the coefficient r (estimated to be about ± 0.04 here). This result, on the one hand, suggests that the inner magnetosphere becomes decoupled from the solar wind if the IMF stays northward for many hours. On the other hand, the correlation with P remains significant, perhaps even more so than it does if the IMF stays southward (smaller r is partially offset by larger N for southward IMF, however).

As far as the specific question is concerned, the answer appears to be negative: a persistently southward IMF does not, over the course of many hours, generate a significantly greater population of energetic O^+ ions at $L < 10$ than does a northward IMF. In fact, the grand averages of all O^+ densities obtained under respective condition are essentially identical.

Table 2. Regression Lines $y = a + bx$, Where $y = \log(AE)$ and $x = \log(P)$ or $x = \log(K)$, All in Terms of Single Hourly Values

Northward IMF ($N = 7386$)		Southward IMF ($N = 7864$)	
$x = \log(P)^*$	$x = \log(K)^*$	$x = \log(P)^*$	$x = \log(K)^*$
$a = 2.48 \pm 0.04$	$a = 3.54 \pm 0.04$	$a = 3.98 \pm 0.03$	$a = 4.16 \pm 0.04$
$b = 0.103 \pm 0.007$	$b = 0.472 \pm 0.012$	$b = 0.309 \pm 0.006$	$b = 0.530 \pm 0.012$
$r = 0.16$	$r = 0.41$	$r = 0.48$	$r = 0.44$

Northward IMF ($N = 7387$)		Southward IMF ($N = 7863$)	
$x = \log(P)^\dagger$	$x = \log(K)^\dagger$	$x = \log(P)^\dagger$	$x = \log(K)^\dagger$
$a = 2.45 \pm 0.04$	$a = 3.49 \pm 0.04$	$a = 4.03 \pm 0.03$	$a = 4.18 \pm 0.04$
$b = 0.104 \pm 0.007$	$b = 0.467 \pm 0.011$	$b = 0.314 \pm 0.006$	$b = 0.528 \pm 0.012$
$r = 0.18$	$r = 0.43$	$r = 0.51$	$r = 0.46$

* P and K from same hour as AE.† P and K from preceding hour.

namely, $0.44 \pm 0.03 \text{ cm}^{-3}$ for northward IMF and $0.44 \pm 0.05 \text{ cm}^{-3}$ for southward IMF.

The energy range of these O^+ data is rather limited, of course, but there is no substantial change in the measured mean energy between the two conditions (not shown) to suggest that O^+ ions outside this range (above or below) change substantially in numbers. By comparison, the grand average hourly AE values during the two sets of O^+ samplings (excluding 1977) are quite different, namely, 82 nT with northward IMF and 341 nT with southward IMF, again a factor 4 apart.

4. Discussion

These O^+ data do not encompass but part of the energy range of magnetospheric O^+ ions, and their spatial coverage of the magnetosphere inside of $23 R_E$ is also incomplete, but they are nonetheless a rather strong indication that the extraction and energization of these terrestrial ions are not a function of the IMF B_z polarity per se. That leaves two fundamental questions: what might be the physical explanation, and why does the O^+ behave differently than the AE index in this regard?

The first question may hinge on the relative importance of kinetic and electromagnetic forces. If the quasi-static solar wind electric field were indeed the primary link, as argued by Lennartsson [1991], it seems improbable that the direction of this field and hence the direction of the IMF B_z (and B_y) would be of no consequence. On the other hand, if the electric field which directly affects the O^+ ions were generated somewhere in the magnetosphere itself, by the kinetic impact of the solar wind particles [e.g., Lundin *et al.*, 1995], then one might not expect a dependence on the direction of B_z . If that were the true mechanism and if this mode of power transfer were nearly linear, then one might instead expect to find the kind of near-linear relationship that is suggested by Table 1 between K and the O^+ .

Except for the fact that it would help explain why the O^+ is not very sensitive to the sign of B_z , there is no conclusive evidence in these data in favor of a mostly kinetic mechanism. The strong mutual correlation between P and K makes their effects hard to separate, and certain aspects of the data, especially the sharp drop in the O^+ density at small angles in Figure 6, suggest that a nonzero electric field is essential, even when the IMF is northward. This latter subject will be revisited later.

In an attempt to view this problem from a different perspec-

tive and to address the second fundamental question, the hourly AE index (see Kamei and Maeda [1981] and subsequent data books) has been correlated with all available hourly values of K and P during the period from January 1, 1978 (no AE for 1977), through March 1, 1980 (end of period covered by the O^+ data). Each AE value has been compared with K and P from same hour, as well as K and P from preceding hours, using a logarithmic representation of each quantity. The correlation has proved to be best with K and P from the same or immediately preceding hour, with a slight edge of the latter. The characteristic parameters of each regression line for those two most recent hours are listed in Table 2.

The AE index, being a gross measure of the total electrojet current, via the magnetic fields from both the eastward and westward electrojets [see Kamei and Maeda, 1981, and references therein], does not by itself represent power dissipation, but if it can be assumed that the resistive properties of the ionosphere do not depend too strongly on current strength, then the square of AE may be a crude proxy. In terms of the logarithmic equation in Table 2 a proportional relationship between solar wind power input and atmospheric power dissipation then requires $b = 0.5$. It is interesting to note that b in fact is very close to 0.5 for the correlation with K (second and fourth columns from left), both with northward (left) and southward (right) IMF, but less so for the correlation with P , especially with northward IMF.

Assuming for a moment that the square of AE is indeed a fair measure of global auroral power dissipation, it is illustrative to rewrite the Table 2 relationship between AE and K from preceding hour as

for northward IMF

$$AE^2 \approx 9.55 \times 10^6 \times K^{0.93} \quad (3a)$$

and

for southward IMF

$$AE^2 \approx 2.29 \times 10^8 \times K^{1.06} \quad (3b)$$

Inserting a typical value of $6 \times 10^{-4} \text{ W m}^{-2}$ for K (approximate grand average in Figure 4) in both of these equations, one finds that the power dissipation is increased by more than a factor of 9 by merely changing the sign of IMF B_z from positive to negative. Why does this not manifest itself more

clearly in the O^+ energy density? Inserting the same K in Table 1 yields less than a factor of 1.8 increase from positive to negative B_z (see also discussion of Figure 7). Actually, if the AE is restricted to times when it has also been preceded by three hours of unidirectional B_z , like the O^+ samplings used in Table 1, the typical difference between northward and southward IMF is more than a factor of 16 in AE^2 (see also discussion of AE in conjunction with Figure 3), that is, about an order of magnitude greater than the increase in the O^+ energy density in the plasma sheet. As implied by previous comments, this difference might even be larger than that in terms of total energies, because the larger O^+ energy density has been sampled from a spatially thinner plasma sheet (sections 3.1 and 3.2).

A plausible resolution of this dilemma is that the AE index reflects not only the true intensity of the electrojet currents but also, perhaps to a much greater extent, the latitudinal distance between these currents and the ground-based observatories. The AE used here was prepared by World Data Center C2, based on magnetograms from 12 stations located, as shown in Figure 1 of Kamei and Maeda [1981], at about evenly spaced longitudes and at geomagnetic latitudes between 60.44° and 71.21° . Being that the northernmost station is at a latitude of only 71.21° , it is far less likely that some station will be in a favorable position to measure the maximum possible H component (south-north and horizontal) from one of the electrojets when the IMF is northward and the auroral oval is contracted, than when the IMF is southward. This may have a strongly biasing effect on the AE (= extreme positive H - extreme negative H), since the H component decays very swiftly with increasing horizontal distance from the current. For example, in the case of an infinitely long and straight-line current at altitude a above a flat surface the H component varies with horizontal distance s as $a^2/(a^2 + s^2)$. With the observer on Earth's curved surface the decay is still swifter. To make a rough estimate, consider the following.

The two categories of IMF direction used in Figures 3 through 7 have average B_z values of $+3.7$ nT and -3.4 nT, respectively. These numbers can be used to infer the corresponding average sizes of the northern auroral oval from Figure 3 in Holzworth and Meng [1975], treating the equatorward edge of the oval as an offset circle (antisunward offset from the magnetic pole). The two radii, in terms of polar angle, are 15.5° and 22° , respectively. With approximate offset angles inferred from Table 1 in that same paper (from quantity A_2), one may estimate that the equatorward edge of the oval, depending on local time, should be at magnetic latitudes Λ_p of

for northward IMF

$$71.5^\circ \leq \Lambda_p \leq 77.5^\circ \quad (4a)$$

and

for southward IMF

$$63^\circ \leq \Lambda_p \leq 73^\circ \quad (4b)$$

If a circular line current is placed along half of the oval at latitude Λ_p , extending symmetrically eastward and westward of the observing station, and at an altitude of 150 km, say, it then follows from (4a), via numerical integration (neglecting field-aligned currents), that the northernmost AE station, at 71.21° , will measure an H component that is between about 0.02 and 0.92 of its maximum (overhead) value (corresponding numbers

for an infinitely long straight-line current 150 km above a flat surface at the same minimum horizontal distance are 0.04 and 0.95). This range contains the factor of 0.25 obtained by dividing the average AE during northward IMF in Figures 3 through 7 with the average AE during southward IMF. Using a line current at the equatorward edge actually amounts to a conservative estimate, since a volume current will have its center further north. It is thus not only plausible but almost certain that (3a) does underestimate the true power dissipation, although it is impossible to determine the precise extent without detailed knowledge of the current distribution, including field-aligned currents.

Now assume instead that auroral power dissipation is independent of the sign of IMF B_z , except perhaps for a short period (order of minutes) of tail reconfiguration following a change in sign [McPherron *et al.*, 1973], and, secondly, that it is proportional to K . If the auroral zone location were purely bimodal, alternating between one poleward and one equatorward position according to the sign of B_z , then one might expect (3a) and (3b) to have an exponent of one on K and only differ in the normalizing factor. However, the latitudinal position of the auroral zones does vary with the magnitude of B_z [Holzworth and Meng, 1975], and if that is taken into account, it may also be possible to explain the varying exponent on K , as well as the Poynting flux effects in Table 2, by the following reasoning.

During times of northward IMF an increase in P causes the polar caps to contract, by means of altered convection, and move the northern electrojets further away from the AE stations, thereby reducing, in effect, both the normalizing factor and the exponent on K , as reflected by (3a). During southward IMF the opposite motion leads to an increase in both numbers, and that is reflected by (3b). In other words, when K and P both increase, in accordance with their mutual correlation (Figure 5), P partially counteracts the driving force of K on the AE index with northward IMF but magnifies this same force with southward IMF. This scenario would explain why the correlation of AE with P is much weaker than with K during northward IMF in Table 2, despite the close mutual correlation between P and K .

This interpretation of the effects of P and K on the AE is further corroborated by invoking again the angle between \mathbf{v} and \mathbf{B} in the solar wind. It was found near the end of section 3.2 that the kinetic energy flux K increases, in a statistical sense, when this angle increases from 0° to 90° (Figure 6, bottom panels), but in terms of relative increase this effect is small compared to the increase in the Poynting flux P , which is due to the fact that P contains the cross product between \mathbf{v} and \mathbf{B} (Figure 6, middle panels). Because of its effect on auroral zone motion, the larger increase in P may thus more than offset the ohmic effect of increasing K on the AE during times of northward IMF. This is indeed the case, as Figure 9 shows. The average AE in the left panels does not actually decrease much with increasing angle (increasing poleward displacement of the northern electrojets), but there is certainly no trace of any statistical increase in K . In the right panels, on the other hand, there is a definitive increase in the average AE, presumably in response to both the reversed auroral zone motion and the increase in K . The average square root of the 1-hour P and K corresponding to the lower right panel of Figure 9 is illustrated in Figure 10.

It is clear from Figures 9 and 10 that the AE does not fall off nearly as sharply with decreasing angle as it would if P were the

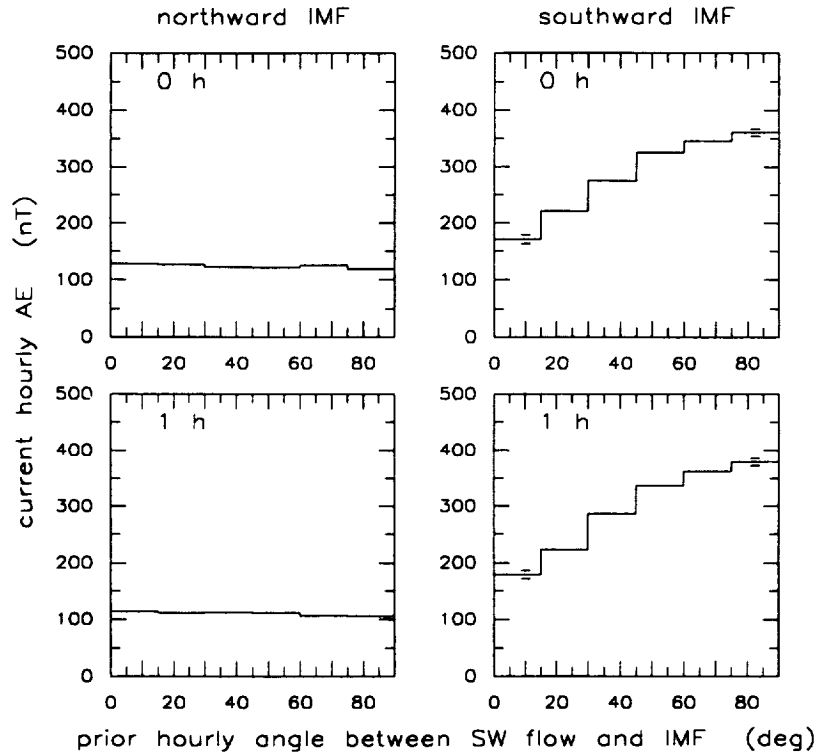


Figure 9. Hourly AE sorted and binned according to the angle between \mathbf{v} and \mathbf{B} in solar wind during (top) same hour or (bottom) immediately preceding hour, when corresponding B_z is (left) northward or (right) southward. These averages include all coincident AE and solar wind data during the time reach of this study (see Table 2 for total number of samplings).

only power source. These figures are based on many more samplings than Figure 6 (see N in Table 2), including well over 300 samplings at angles below 15° in each panel. The left and right panels of Figure 9 together suggest that the AE has an average value somewhat above 100 nT at zero angle. The corresponding currents, which may in fact be larger than this measure would suggest, can thus be maintained without a solar wind electric field ($\mathbf{v} \times \mathbf{B} = 0$). It is worth keeping in mind that this is an average level; there are numerous (hourly) samplings at near-zero angle with substantially larger AE, as well as lower values, no doubt reflecting the variation in K . This is illustrated by the least squares fits in Table 3.

The fact that the AE in the right panels of Figure 9 falls off faster with decreasing angle than the square root of K does in Figure 10 must be viewed against the expected poleward motion of the electrojets. Using again the results of *Holzworth and Meng* [1975], one would expect the equatorward edge of the oval, depending on local time, to be somewhere in the latitude range of 67° to 75° with zero angle between \mathbf{v} and \mathbf{B} (zero B_z). This is already a less than ideal location for AE measurements, especially since the electrojets extend northward of this edge.

Judging from the AE index alone, it thus seems quite possible that K is indeed the dominant external source of power for the auroral processes and that P has mainly a modulating influence on the auroral zone position. This subordinate role of P , which is consonant with its minuscule contribution to the total solar wind energy flux, may still allow it to serve as a trigger of substorms, by inducing, now and then, the release of internal tail energy [e.g., *McPherron et al.*, 1973] previously supplied by K . This scenario would help explain why the O^+ is

rather independent of the IMF B_z polarity. However, it does not explain why, in Figure 6, the O^+ density (top panels) appears to go to zero when the electric field vanishes.

This peculiar difference between the O^+ and the AE, if real (see last paragraph of section 3.2), may reflect a spatial difference between the electrojets and the ionospheric O^+ source. It is possible, considering other O^+ measurements from closer to Earth and at lower energies, that the O^+ source, unlike the electrojets, is concentrated to the dayside portion of the auroral zones, perhaps even to a narrow sector about local noon [*Moore et al.*, 1986]. A dayside or, more appropriately named, sunlit source for plasma sheet O^+ ions may even be easier than a nightside one to reconcile with the strong dependence of these ions on variations in the solar EUV radiation [*Lennartsson*, 1991]. If the extraction of O^+ ions near noon can be assumed powered by the direct penetration of solar wind kinetic energy flux K through the geomagnetic cusps, then it can perhaps be argued that the extraction is somehow mechanically inhibited when the IMF is parallel to the solar wind flow. Although a pure speculation at this time, this line of reasoning might offer an alternative explanation for the sharp decrease in the O^+ density at small angles in Figure 6, one that does not invoke the solar wind electric field per se.

5. Concluding Remarks

In view of these new results it appears that the original conclusions by *Lennartsson* [1991] were incomplete and possibly wrong in part. In particular, the good correlation that was found between the solar wind electric field and the plasma

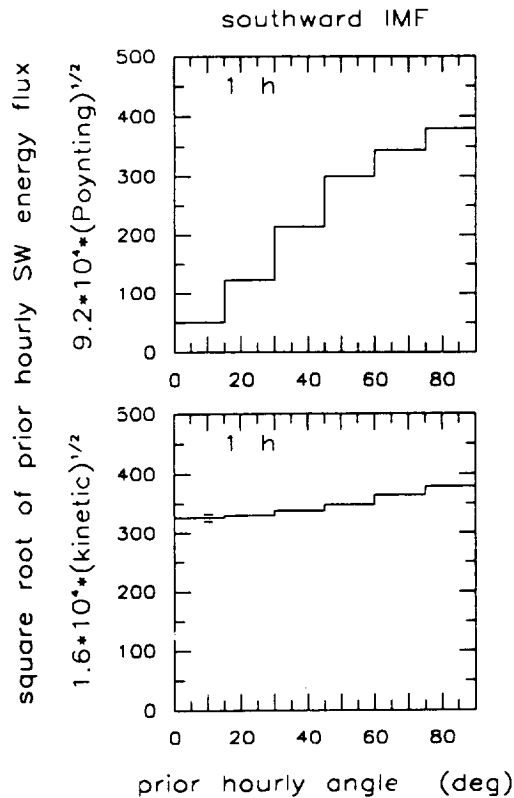


Figure 10. Averages of the square root of each hourly (top) P and (bottom) K corresponding to the lower right panel of Figure 9, normalized to the same maximum value as the AE.

sheet O^+ density does not necessarily imply a close physical link between those two quantities; it may be due to the strong mutual correlation between the Poynting flux P and the kinetic energy flux K in the solar wind (Figure 5), and K may be what provides the strongest physical link. It is certainly clear, at least, that the original study gave inadequate consideration to the kinetic aspects.

The new results do confirm the original finding that the plasma sheet O^+ population is rather insensitive to the polarity of the IMF B_z , but they also suggest a reason for that effect which would contradict one of the original conclusions: the solar wind electromagnetic energy flux P is a less important power source for the extraction and energization of O^+ ions, and perhaps for auroral processes in general, than is the kinetic energy flux K . The modest increase (less than a factor of 2) in the typical O^+ energy density during times of southward IMF may not be due to enhanced transmission of P but rather to recent and transient release of energy previously supplied by K .

Table 3. Regression Lines $y = a + bx$. Where $y = \log$ (AE) and $x = \log$ (K), and Angle Between v and B Limited to $<15^\circ$

K From Same Hour as AE ($N = 657$)	K From Preceding Hour ($N = 657$)
$a = 3.8 \pm 0.2$	$a = 3.9 \pm 0.2$
$b = 0.51 \pm 0.05$	$b = 0.53 \pm 0.05$
$r = 0.40$	$r = 0.42$

and stored in the tail [e.g., Hones et al., 1971; McPherron et al., 1973]. The significance of P may lie in its role as a trigger of tail reconfiguration. That is, P may supply the relatively small power required to "pull the trigger," when B_z changes from northward to southward [McPherron et al., 1973], but to "hold back the trigger," by keeping B_z negative for many hours, as done in Figure 8, may not have much effect on subsequent events.

It is often thought that the expansion of the auroral ovals following a southward turning of the IMF implies that energy is being "loaded" into the tail [e.g., McPherron et al., 1973], but that need not be the case if the lobes expand at the expense of the particle content of the thinning plasma sheet [e.g., Hones et al., 1971; Lennartsson and Shelley, 1986]. That is, the sum of magnetic and kinetic tail energies may not increase, unless K also increases.

If the plasma sheet O^+ energy density is taken to be a good cumulative measure of recent auroral power dissipation, it then follows that the strong IMF B_z dependence of the AE index needs to be reevaluated; it may be caused in part by the northern electrojets moving into and out of the latitudinal range of the AE magnetometers. The crude comparison made above between line currents at different latitudes provides an additional and independent argument why this effect might be significant. This applies mainly to the hourly AE, which reflects some of the cumulative effects of currents, by virtue of being an average over time, but may not properly account for more rapid (order of minutes) variations at substorm onset.

This interpretation does have attractive simplicity, but it may or may not be compatible with the observed sharp reduction in the plasma sheet O^+ density when the solar wind v and B become nearly parallel (Figure 6, top panels). It may be possible, as speculated above, to explain this effect without invoking the solar wind electric field, and the effect might even be a statistical artifact (last paragraph of section 3.2), but it is probably prudent to keep an open mind about the exact role of this field until the subject has been studied in greater depth.

Acknowledgments. The author wishes to thank H. L. Collin for helpful discussions and for his assistance in preparing computer plotting routines, W. K. Peterson for his initial efforts to make these data accessible on the Internet, and two referees for their many insightful comments. The author is also indebted to C. T. Russell for the use of ISEE 1 magnetometer data, to the National Space Science Data Center for providing magnetic tape records of the IMF and solar wind data, and to the National Oceanic and Atmospheric Administration for providing similar records of geophysical indices. This work was supported by NASA under contract NASW-4816.

The Editor thanks E. Möbius and another referee for their assistance in evaluating this paper.

References

- Balsiger, H., P. Eberhardt, J. Geiss, and D. T. Young, Magnetic storm injection of 0.9- to 16-keV/e solar and terrestrial ions into the high altitude magnetosphere, *J. Geophys. Res.*, **85**, 1645, 1980.
- Bevington, P. R., *Data Reduction and Error Analysis for the Physical Sciences*, McGraw-Hill, New York, 1969.
- Couzens, D. A., and J. H. King, Interplanetary medium data book, supplement 3, 1977-1985, *Rep. NSSDC/WDC-A-R&S 86-04*, NASA Goddard Space Flight Cent., Greenbelt, Md., 1986.
- Daglis, I. A., S. Livi, E. T. Sarris, and B. Wilken, Energy density of ionospheric and solar wind origin ions in the near-Earth magnetotail during substorms, *J. Geophys. Res.*, **99**, 5691, 1994.
- Fairfield, D. H., and N. F. Ness, Configuration of the geomagnetic tail during substorms, *J. Geophys. Res.*, **75**, 7032, 1970.
- Ghielmetti, A. G., R. G. Johnson, R. D. Sharp, and E. G. Shelley, The